LA-UR -81-2867

MASTER

CONF-810641--16

TITLE: SYSTEMATICS OF RADII AND NUCLEAR CHARGE DISTRIBUTIONS INDUCED FROM ELASTIC ELECTRON SCATTERING, MUONIC X-RAY, AND OPTICAL ISOTOPE-SHIFT MEASUREMENTS

AUTHOR(S): H. J. Emrich, G. Fricke, M. Hoehn, K. Kaser, H. Miska, B. Robert-Tissot, D. Rychel, L. Schaller, L. Schellenberg, H. Schneuwly, B. Shera, H. G. Sieberling, R. Steffen, H. D. Wohlfahrt, Y. Yamazaki

SUBMITTED TO: "Fourth International Conference on Nuclear Far from Stability" Helsingor, Denmark, 7-13 June 1981. Invited paper.

DISCLAIMER

By acceptance of this article, the publisher recognizes that the U.S. Government retains a nonexclusive, royalty-free license to publish or reproduce the published form of this contribution, or to allow others to do so, for U.S. Government purposes.

The Los Alamos National Laboratory requests that the publisher identify this article as work performed under the auspices of the U.S. Department of Energy.

University of California

LOS ALAMOS NATIONAL LABORATORY

Post Office Box 1663 Los Alamos, New Mexico 87545

An Affirmative Action/Equal Opportunity Employer

Form No. 836 R3
St. No. 2629
12/78

UNITED STATES
DEPARTMENT OF ENERGY
CONTRACT W-7405-ENG-36

(Invited paper) presented at
"4th International Conference on Nuclei Far from Stability"
Helsingør, Denmark, 7-13 June 1981

SYSTEMATICS OF RADII AND NUCLEAR CHARGE DISTRIBUTIONS DEDUCED FROM ELASTIC ELECTRON SCATTERING, MUONIC X-RAY AND OPTICAL ISOTOPE SHIFT MEASUREMENTS

H.J. Emrich[+)], G. Fricke[+)*], M. Hoehn[+++)], K. Käser[++)], M. Mallot[+)], H. Miska[+)], B. Robert-Tissot[++)], D. Rychel[+)], L. Schaller[++)], L. Schellenberg[++)], H. Schneuwly[++)], B. Shera[+++)], H.G. Sieberling[+)], R. Steffen[++++)], H.D. Wohlfahrt[+++)], Y. Yamazaki[+++)]

[+)] Institut für Kernphysik, Universität Mainz, Mainz, Germany

[++)] Institut de Physique de l'Université de Fribourg, Pérolles, Fribourg, Suisse

[+++)] Los Alamos Scientific Lab., University of California, Los Alamos N.M., U.S.A.

[++++)] Department of Physics, Purdue University, Lafayette Indiana, U.S.A.

Abstract

The nuclear charge distribution and nuclear charge distribution differences have been investigated by 250 MeV elastic electron scattering at the Institut für Kernphysik, Universität Mainz.

Muonic X-ray measurements yield complementary information to electron scattering results. Both experimental data are analysed in an almost model independent way. Muonic X-ray measurements have been performed for the region [illegible] up to [illegible] Mo.

Muonic X-ray transition energies allow the determination of the radial parameter h, - the Barrett radius - with high precision. This Barrett radius combined with the charge distribution from elastic electron scattering yields the following precise radial parameters [illegible] and [illegible]. With the absolute values of these radial parameters it is possible to determine the two critical constants: the electron density at the nucleus and the specific mass shift. Thus the isotopic and isotone shift data from the optical region yield the absolute values of these shift [illegible]. Therefore it will be also possible to [illegible] the RMS-radii of isotopic nuclei with good accuracy.

The differences in RMS-radii between isotopes and isotones show systematic trends with a strong shell effect. As one example one observes that the differences in radii are largest at the beginning of a neutron shell and decrease linearily to the end of a shell. Experimental results will be compared with theoretical Hartree-Fock calculations and the influence of the quadrupole deformation [illegible]. Data of odd mass staggering effects on isotopes and isotones will be discussed in the [illegible] and [illegible] regions. Some differences of charge distributions will also be presented.

1. Introduction

Detailed knowledge of the rearrangement of the nuclear charge distribution in response to the addition of neutrons in the [illegible] of a whole series of isotopes [illegible] a challenging test of one's understanding of the structure of nuclear ground states.

In this collaboration of the laboratories of Mainz, Los Alamos and S.I.N.-Fribourg a systematic survey is being performed of all stable isotopes and isotones in the region between [illegible] Ca to [illegible] Mo. It is the goal of these experiments to determine nuclear charge distributions and accurate differences of nuclear charge distributions between neighbouring nuclei.

These quantities are determined by high energy elastic electron scattering measurements - up to 350 MeV at the Mainz University [illegible] - and by muonic X-ray studies: the region [illegible] to [illegible] at Los Alamos ([illegible]) and the region [illegible] to [illegible] at S.I.N.([illegible]). All the latter data are not yet published and are to be regarded as preliminary.

Elastic electron scattering yields information about the charge distributions and charge distribution differences. Elastic scattering data essentially determine the Fourier transform of the nuclear charge distribution, [illegible] even in the [illegible] of a phase shift analysis. Therefore, the measurements determine directly the nuclear charge distributions and charge distribution differences, provided the measurements are [illegible] and extend over a sufficiently large range [illegible] transform. By using a Fourier-Bessel [illegible] the elastic error band [illegible] for the charge distributions and their differences, which [illegible] both the statistical [illegible] and the [illegible] limited range of measured momentum transfer [illegible]. For example fig. 1 shows the charge distribution [illegible] with the correlated errors.

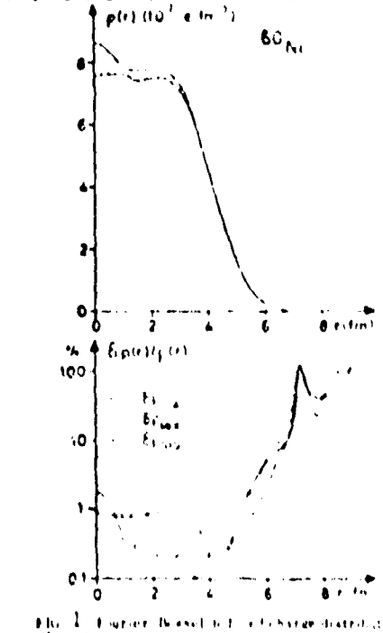

Fig. 1 Fourier Bessel [illegible] charge distribution of [illegible]. The error band [illegible] the [illegible] and [illegible] momentum transfer [illegible] and [illegible] the [illegible]

*) presented by G. Fricke

Muonic data, on the other hand, determine one integral quantity like the Barrett radial moment $\langle r^k e^{-\alpha r}\rangle$ of the nuclear charge distribution[10]. As an example for Ni, Z=28, k=2,12 and α=0,076 fm^{-1}. The precision of the muonic data is almost 5-10 times better compared with elastic electron scattering radii. To compare these results with optical isotope shift data, one needs the radial moments $\langle r^n\rangle^{1/n}$ with n=2,4,6. A combination of electron scattering data with the muonic X-ray measurements allows one to determine the even radial moments with almost the same precision as the Barrett radius. With the knowledge of these radial moments from three isotopes it is possible to extract the two constants of the optical isotope shift measurements: the density of the electron at the nucleus and the specific mass shift.

With an absolute calibration of these two optical constants, the absolute values of the RMS-radii of long chains of optical isotope shift measurements from the off stability region are available: e.g. Hg, Ba, Rb, Cs a.s.o. .

The results of these three methods can be interpreted entirely on the basis of electromagnetic interaction and exhibit; therefore, the following advantages exist:

a) Since the electromagnetic interaction is exactly know, an accurate determination of nuclear structure properties is possible.

b) Compared with the nuclear forces the electromagnetic interaction is weaker, therefore in these experiments the distortion of the nuclei to be measured can be accounted for by only small correction terms.

The older muonic atom data and elastic electron scattering data could be described in good approximation with a two parameter Fermi charge distribution. By assuming a constant surface thickness and constant central density, the equivalent radii of a homogeneously charged sphere deduced from the RMS radii of the above Fermi distributions were represented by the following A-dependence:

$$R_{eq} = 1.12\ A^{1/3} + 0.009A^{-1/3} - 1.513A^{-1} \qquad (1)$$

in good agreement with the experiments[11].

In the present paper results are reported from muonic X-ray and elastic electron scattering measurements in the region Ca-Mo. The experiments clearly show systematic effects of the shell structure, which will be discussed.

2. Muonic X-Ray Measurements

The experimental apparatus and the procedure to measure and extract nuclear charge parameters from muonic isotope and isotone shifts are described in detail in the paper of E.B. Shera[9]. Nevertheless, some remarks and definitions may be useful. The muon binding energy of adjacent nuclei differ slightly from each other due mainly to two effects: the difference in the mass (which can be accounted for by the reduced mass), and the size of the charge distribution ("field shift"). The "field shift" has been used to determine differences in the nuclear radii.

The "field shift" difference for spherical charge distribution differences $\delta\rho(r)$ is given by

$$\Delta E = Z^2 \int \delta\rho(r)\,[V_\mu^{2p}(r) - V_\mu^{1s}(r)]\,d\tau, \qquad (2)$$

where $V_\mu^{2p}(r)$ and $V_\mu^{1s}(r)$ are the potentials generated by the 2p and 1s bound muons, respectively.

To extract a "model independent" radius, the procedure proposed by Barrett[10] has been used. Barrett has shown that the potential difference in eq. (3) can be approximated by

$$V_\mu^{2p} - V_\mu^{1s} = A + Br^k e^{-\alpha r} \qquad (3)$$

which demonstrates that the quantity

$$\langle r^k e^{-\alpha r}\rangle = \int \rho(r) r^k e^{-\alpha r} d\tau \qquad (4)$$

is model independent within the experimental error.

The value of k in this equation is different for different transitions and also varies slowly as a function of Z for a given transition. The value of α varies linearly with Z and is usually kept fixed for all transitions of one element (for example ^{70}Zn: α=0,079 fm^{-1}, k=2.130).

An equivalent radius - the "Barrett" radius R_B - can be defined by equating this quantity with the corresponding quantity of an uniformly charged sphere of radius R_B:

$$3R_B^{-3}\int_0^{R_B} r^k e^{-\alpha r} r^2 dr = \langle r^k e^{-\alpha r}\rangle \qquad (5)$$

The data in this paper are given without errors and are preliminary. After a careful analysis, the experimental error for R_B will be in the order of $\pm 1\cdot 10^{-3}$fm, whereas the uncertainties due to theoretical corrections (for the most part nuclear polarization) is $\pm 5\cdot 10^{-3}$fm. The theoretical error for radius differences reduces to $\pm 1\cdot 10^{-3}$fm.

3. High Energy Elastic Electron Scattering

Though this method is well known and has been described before, it is worthwhile to summarize a few important facts[12-14]:

The elastic electron scattering cross section in first order Born approximation is given by

$$\frac{d\sigma}{d\Omega}(E_0, \theta) = \frac{d\sigma}{d\Omega}_{Mott} \cdot F^2(q^2). \qquad (6)$$

$\frac{d\sigma}{d\Omega}_{Mott}$ describes the point charge cross section.

For spherical, I=0, nuclei the nuclear form factor is given by

$$F(q^2) = 4\pi\int_0^\infty \rho(r)\frac{\sin(qr)}{qr} dr \qquad (7)$$

where q stands for the momentum transfer $q = (2E_0/\hbar c)\sin\theta/2$.

A variation of the momentum transfer q can be achieved by variation of either the incoming electrons E_0 or of the scattering angle θ. This results in a variation of the weighting function sin (qr)/qr for the charge distribution in the nuclear form factor. The electron scattering experiments covered a range of q: 0,5fm^{-1}<q<2,5fm^{-1}, which allows one to resolve structures of the nuclear charge distributions in the order of the proton diameter.

The evaluation of the nuclear ground state charge density from the scattering data has been performed by an almost model independent method

described in detail by B. Dreher et al.(9).

The 350 MeV experimental electron scattering setup of the Mainz University has the following facilities: In order to measure small charge distribution differences of isotopes or isotones, the targets are mounted on a wheel, which allows a fast automatic target chang . This method reduces most of the experimental uncertainties to below the level of the statistical error(14).

The intensity of the incident electron beam is monitored by a ferrite-transformer(15,16) and a Faraday-cup. At the same time, a second fixed angle spectrometer monitors the product of electron current and target thickness. The resulting accuracy for charge distribution differences can be seen in Fig. 12.

From the charge distribution determined by elastic electron scattering, it is possible to deduce the ratio of the RMS-radius to the Barrett-radius with a precision comparable of that of the Barrett-radius, measured by muonic X-ray experiments. This is caused by the fact that the two radial moments are quite similar. In this way it is possible to extract the radial moments from elastic electron scattering and muonic X-ray data with almost the same precision with which the Barrett radius is known. We will use these precise radial moments to calibrate the optical isotope shift data.

4. Optical isotope shifts and [illegible]

The isotope shift $\delta\nu_{exp}^{A,A'}$ between two isotopes with mass number A and A' observed in the wave number ν is the sum of the field shift and the mass shift, according to the following formula:

$$\delta\nu^{A,A'} = c\Delta|\psi(0)|^2_{elec}\,[\langle r^2\rangle + c_1\langle r^4\rangle + c_2\langle r^6\rangle + \ldots]$$

$$+ \frac{A'-A}{A\cdot A'}\cdot M_{mass\ shift}$$

The density of the electron at the nucleus given by $\Delta|\psi(0)|^2$ is only approximately known. Also, the mass shift contains a contribution from the specific mass shift, which is not well known either. If one knows the absolute radial moments $\langle r^2\rangle^{1/2}$, $\langle r^4\rangle^{1/4}$ and $\langle r^6\rangle^{1/6}$ with high precision from elastic electron scattering and muonic X-ray data, then it is possible to deduce the above mentioned two constants. These two constants should not be dependent on the isotope, so it will be possible to extract the absolute RMS radius of isotopes far from the region of stability. The great precision of today's laser spectroscopy and collinear fast beam laser spectroscopy allows the determination of the difference in the RMS-radii with an error less than 0.5·10⁻³ fm. Some examples will be given in the talk of Dr. Otten.

The relative contribution of the higher radial moments $\langle r^4\rangle^{1/4}$ and $\langle r^6\rangle^{1/6}$ is plotted in Fig. 2.

Contribution of higher radial moments to Optical I.S.

$$\delta\nu_{exp}^{A,A'} = \Delta|\psi(0)|^2\cdot\underbrace{[\delta\langle r^2\rangle + c_1\delta\langle r^4\rangle + c_2\delta\langle r^6\rangle + \ldots]}_{\lambda} + \text{mass-shift}$$

$\langle r^2\rangle^{1/2}$; $\langle r^4\rangle^{1/4}$; $\langle r^6\rangle^{1/6}$ deduced from (e,e) and μ-atom

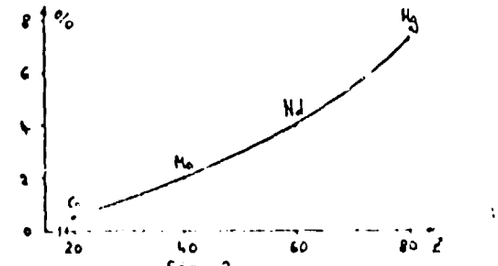

Fig. 2

For example, the mercury field shift measurement contains a contribution of about 7.5 % from the higher radial moments. Fig. 3 shows a King-plot of optical isotope shift measurements against muonic X-ray data.

Hg Isotope

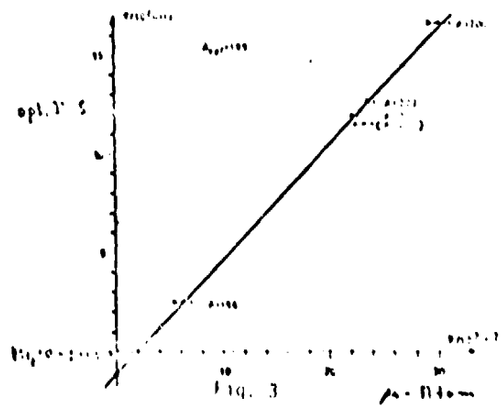

Fig. 3

The shift of 20 Hg is not included. It may be that this value has a systematic error. The spectroscopic constant is found to be (-17,4 ± 2,9) GHz·fm². This is approximately 27 % larger than the constant given by Bonn et al.(17). The specific mass shift determined by the King-plot is 14 times larger than the normal mass shift but with an error of about 70 %. The odd stable isotopes of mercury have been remeasured recently at Los Alamos by P. Sheri et al. but are not yet published. If these new data are available, the two optical constants can be certainly determined with higher precision.

5. Results, Systematics and Interpretation of Differences of RMS Radii

5.1 Isotope shifts

The aim of this experiment has been to study the systematics of differences of RMS-radii for isotopes and isotones. Results for Fe, Ni, Cu and Zn isotopes have been already published(5,6). These measurements were extended to the $1f_{7/2}$ shell nuclei(7), the nuclei near the closed N=50 shell and the N=56 subshell(8). The results are shown in Fig. 4 where the differences in the RMS-radii of isotopes from Ca to Mo for ΔN=2 are plotted.

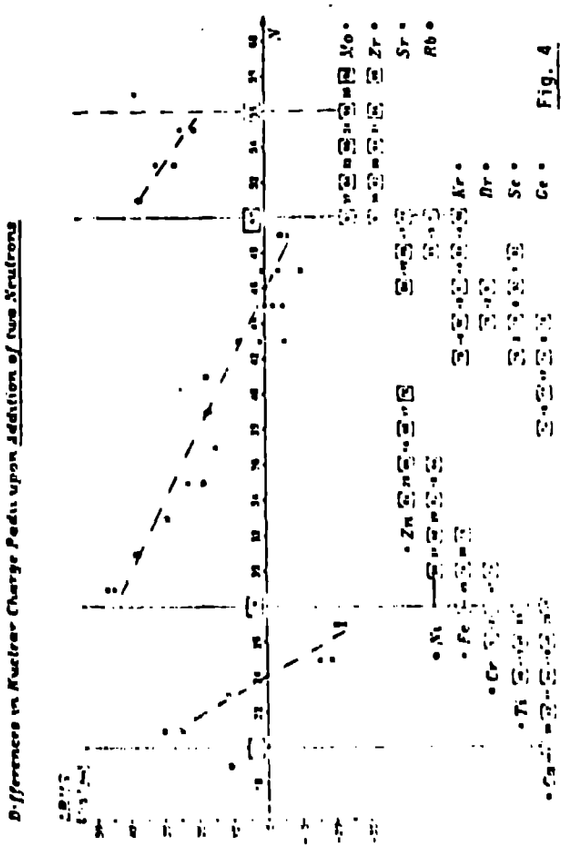

Each isotope is represented by a square with the mass number A. The figures between the squares indicate the differences in the RMS-radii between neighbouring isotopes. The results are plotted against the neutron numbers.

The radii differences between even isotopes ΔN=2 due to the proton core polarisation by the added two neutrons, indicate strong systematic shell effects (Fig. 4).

a) The addition of the first two neutrons in the $1f_{7/2}$ neutron shell e.g. ^{40}Ca - ^{42}Ca or ^{40}Ar - ^{42}Ar show a strong increase of the radius. The same is seen after the closed neutron shell N=28 between ^{56}Fe - ^{54}Fe or ^{56}Ni - ^{58}Ni. This occurs also after N=50 or N=56. A sequential addition of neutron pairs in the different shells shows in Fig.4 results in an almost linear decrease in the successive isotope shifts.

b) Furthermore, it is apparent that the isotope shifts are independent of the proton configuration of the nucleus involved,(e.g. the ^{58}Fe-^{56}Fe and ^{60}Ni-^{58}Ni isotope shifts are identical within the experimental uncertainties). We find this behavious quite remarkable, particularly in the view that the proton configuration of Ni is magic Z=28. At the end of the $1f_{7/2}$ shell and the $1g_{9/2}$ shell, one observes that the radius becomes smaller upto an addition of two neutrons e.g. ^{48}Ca-^{46}Ca the RMS radius becomes $20 \cdot 10^{-3}$fm smaller. The same can be seen for the Sr, Rb and Kr-isotopes. By adding four times in sequence two neutrons to fill the $1g_{9/2}$ shell, the RMS radius of the Kr-isotopes is becoming always smaller. In the $2d_{5/2}$ subshell a decrease of the radius by adding the last two neutrons does not occur.

c) A sudden increase in the isotope shifts occurs at N = 20,28,50 and 56.

d) At the beginning of a new neutron shell, the independence of the proton configuration is stronger compared to the end of the neutron shell.

In the following figures (5-9)

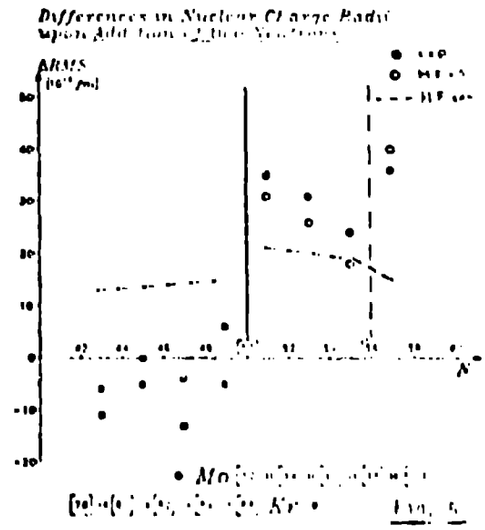

Differences in Nuclear Charge Radii upon Addition of two Neutrons

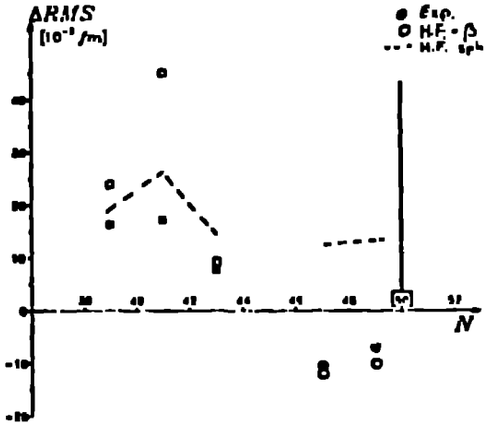

[84] → [86] → [88] Sr •

[70] → [77] → [74] → [76] Ge •

Fig. 6

Differences in Nuclear Charge Radii upon Addition of two Neutrons

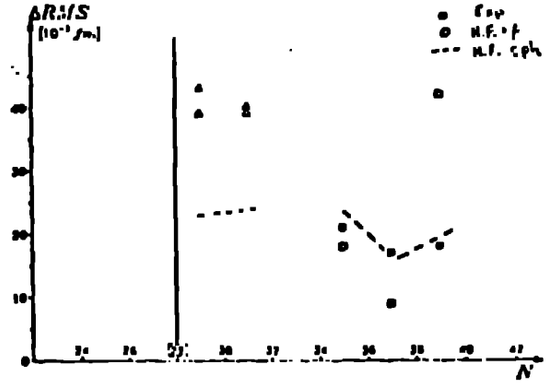

• Zn [64] → [65] → [68] → [70]

▲ Fe [54] → [56] → [58]

Fig. 8

Differences in Nuclear Charge Radii upon Addition of two Neutrons

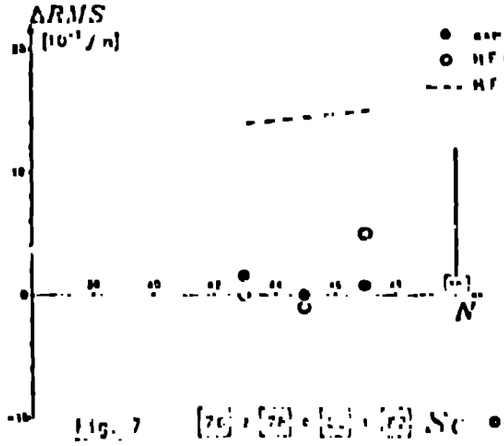

Fig. 7 [76] → [78] → [80] → [82] Se •

we compare the experimental results with spherical Hartree-Fock-calculations from Reinhard and Drechsel taking into account experimental B(E2) values to the lowest 2+ states. The H.F. term makes a smoothly varying and almost constant contribution to the differences of the RMS-radii. The B(E2)-related term, which is identical to the corresponding term in the usual incompressible fluid model formulation, introduces a strong variation in the predictions for different isotopes. The deviation seems to be within a range of $15 \cdot 10^{-3}$fm, except for the Ca-isotopes, where the inclusion of octupole deformations improves the result. The agreement between experiment and theorie is, of course, limited by the error of the measured B(E2) values.

The differences of the RMS-radii for the isotopes of ^{32}Ge up to ^{38}Sr at the end of the $1g_{9/2}$ neutron shell in the region N=50 is given in Fig.10.

Differences in Nuclear Charge Radii upon Addition of two Neutrons

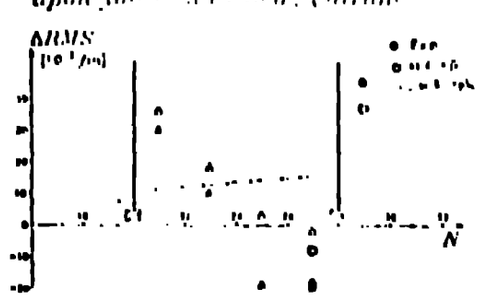

• Cr [50] → [52] → [53]

▲ Ca [40] → [42] → [44] → [46] → [48]

Fig. 9

Differences in Nuclear Charge Radii upon Addition of two Neutrons

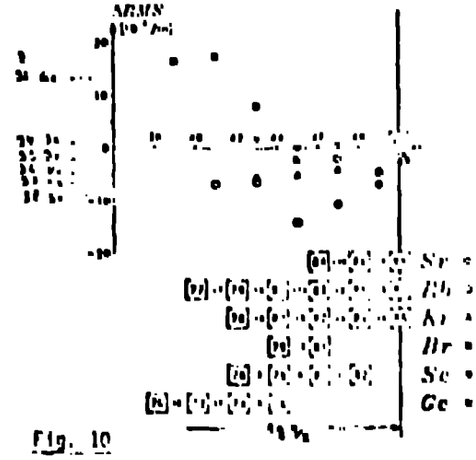

[84] → [86] → [88] Sr •

[77] → [79] → [81] → [83] → [85] → [87] Rb •

[78] → [80] → [82] → [84] → [86] Kr •

[79] → [81] Br •

[78] → [80] → [81] → [82] Se •

[76] → [77] → [78] → [80] Ge •

Fig. 10

Here the Z-independence of the change in the RMS-radii seems to be less pronounced compared to the beginning of the neutron shell. The average value for each element - as indicated at the left side of Fig. 10 - shows a systematic tendency that the ΔRMS-radius becomes smaller with increasing Z.

5.2 Isotone shifts

The sequential addition of proton pairs after Ca (Z=20) and Ni (Z=28), shown in Fig. 11 results in an almost linear decrease in the successive isotone shifts.

Differences in Nuclear Charge Radii upon Addition of two Protons

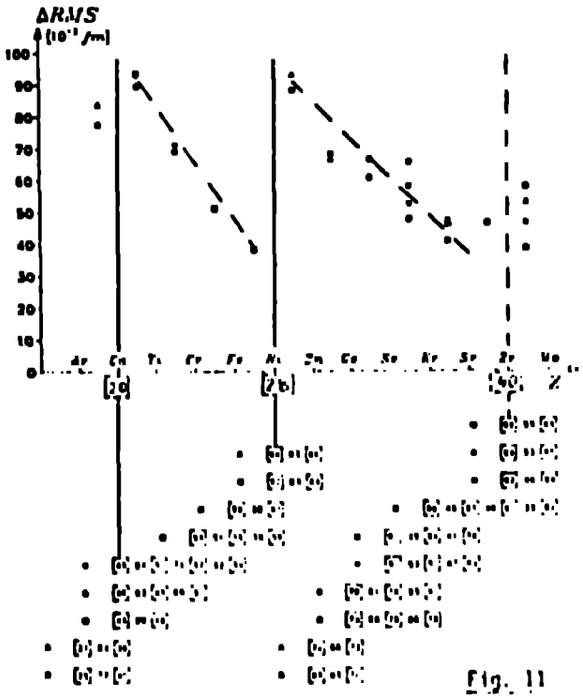

Fig. 11

Furthermore, it is apparent that the isotone shifts are independent at the neutron configuration of the nuclei involved, especially for the $1f_{7/2}$ proton shell nuclei Ca to Ni. For example, the ^{46}Ti-^{44}Ca, ^{48}Ti-^{46}Ca and ^{50}Ti-^{48}Ca isotone shifts are all identical and not dependent on, e.g., double magic nuclei like [illegible] or the not magic nuclei [illegible]. A sudden increase in the isotone shifts, more than a factor of two occurs at Z=28, while neutron-configuration independence is maintained. In this case, the sudden increase reflects the beginning of the $2p_{3/2}$ proton shell. In Fig. 12 the differences in the charge distribution - measured by elastic electron scattering - show clearly the further radial extension of the $2p_{3/2}$ proton wave functions compared to the $1f_{7/2}$ proton wave functions.

The isotone ΔZ=2 RMS-radii differences before and after the magic neutron number N=50, (see Fig. 13), seems to be in a systematic way larger than at N=50. In Fig. 14, around N=28, this effect cannot be observed.

It is interesting to see the similarity of the systematic [illegible] shifts.

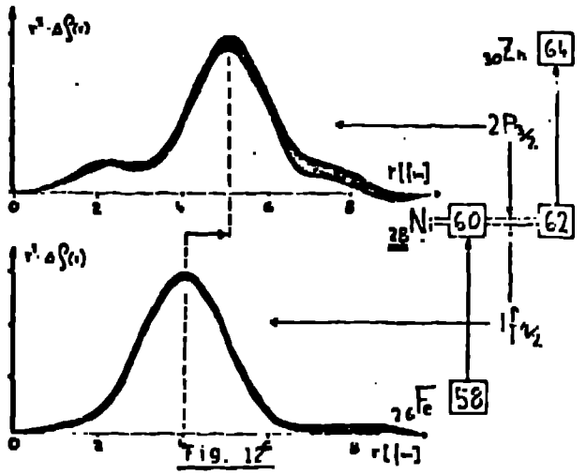

Fig. 12

Isotone ΔZ=2 Radii Differences around N=50

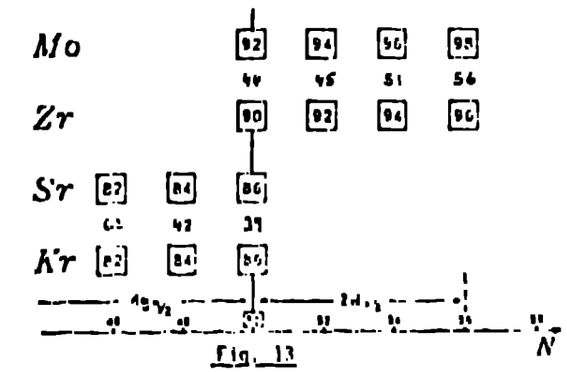

Fig. 13

Isotone ΔZ=2 Radii Differences around N=28

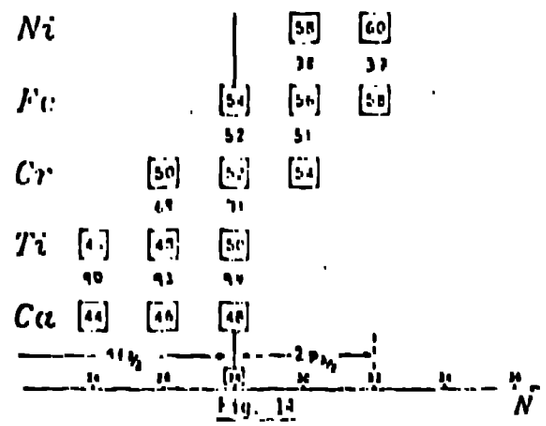

Fig. 14

5.3 Comparison of isotone and isotope shifts and core polarisation effects

Isotone shifts, in contrast to isotope shifts, are dominated by the charge of the added protons. Thus, before isotope- and isotone-shift data can be compared on an equivalent basis, the charge distribution of the added protons must first be considered. Elastic electron scattering experiments -Fig. 12- have shown that the radial dependence of $\Delta\rho(r)$ between $1f_{7/2}$-shell isotones is well described by $1f_{7/2}$-shell harmonic oscillator wave functions. As a zeroth-order approximation, we therefore calculated a set of $1f_{7/2}$-shell isotone shifts considering only the charge distribution of the added protons. In Fig. 15 the experimental isotone shifts are compared with a harmonic oszillator shell model calculation.

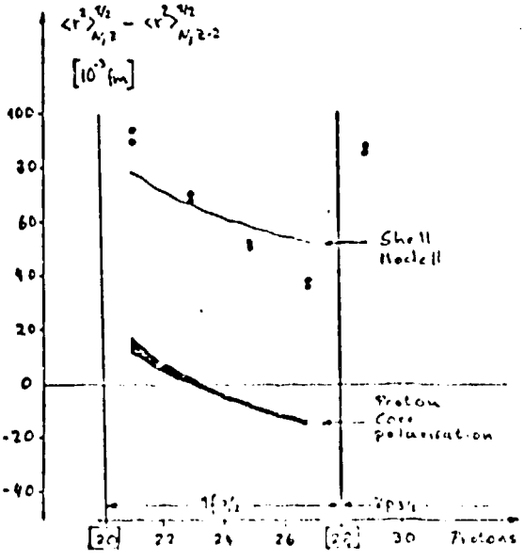

Fig. 15

The actual isotone shifts decrease more rapidly with increasing Z than the calculation would suggest.

It is evident that the effect of the added nucleons on the proton core must be included when considering either isotone or isotope shifts. In the case of isotope shifts, this "core polarisation" is the only effect between N=28 and N=28, (see Fig.4). The difference between the measured isotone shifts and the contribution of the proton charge should be the proton produced core polarisation, (see Fig. 15). This proton core polarisation is positiv in the first half of the $1f_{7/2}$ proton shell and negative in the second half. The core polarisation caused by the added neutrons, as seen in Fig.4, is in the average about two times stronger than the proton produced core polarisation. We conclude that the proton- and neutron-core polarisation reveal qualitatively a similar behaviour in the $1f_{7/2}$ shell.

5.4 Isotone and Isotope odd-even staggering

Around N=50 Fig.16 displays the odd-even staggering for isotones and isotopes. The increase of the RMS-radius due to the first unpaired nucleon is smaller compared to the effect of the second nucleon; this is shown for neutrons and protons.

Isotone and Isotope Odd-Even Staggering

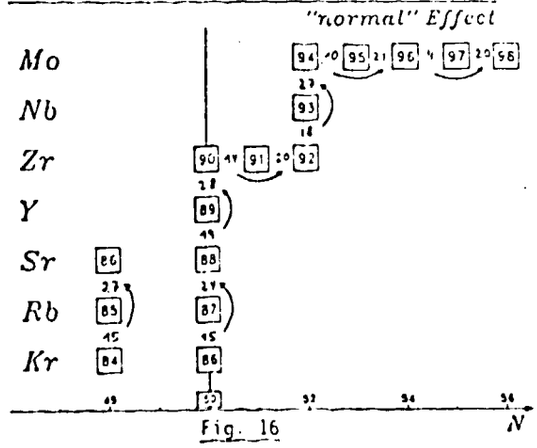

Fig. 16

This may be called the "normal" odd-even staggering effect. Reehal and Sorenson predict smaller deformations for odd then for even isotopes, because ground state correlations are blocked by the unpaired nucleon(18). The arrow in Fig.16 indicates the direction from smaller to larger increase of the RMS-radius. In Fig.17, the isotope odd-even staggering around N=28 shows for N=28 a "normal" effect. The isotone effect is "normal" below Z=28, but for Z=28 the first proton (^{63}Ca-^{62}Ni) yields almost the same increase of the RMS-radius as the second proton (^{64}Zn-^{63}Cu) in the new $2p_{3/2}$ proton shell. The Ca isotope shift in the first half of the $1f_{7/2}$ shell is "normal", whereas in the second half of the $1f_{7/2}$ shell the Ca and Ti shifts for the first added neutron (^{45}Ca-^{44}Ca; ^{47}Ti-^{46}Ti) is larger in the amount of the difference of the RMS-radius compared to the effect of the second neutron (^{46}Ca-^{45}Ca; ^{48}Ti-^{47}Ti). The "normal" odd-even staggering effect in the first half of the $1f_{7/2}$ neutron shell may be explained by the increasing deformation and the "not normal" effect in the second explained by the decreasing deformation. The details of this behaviour, however, may not be easy to explain.

Isotone and Isotope Odd-Even Staggering

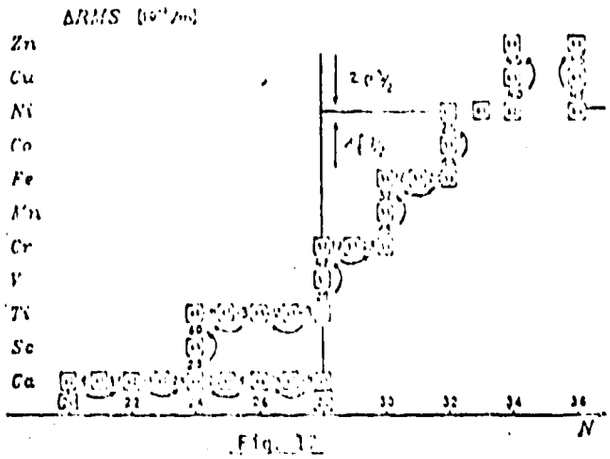

Fig. 17

5.3 Comparison of isotone and isotope shifts and core polarisation effects

Isotone shifts, in contrast to isotope shifts, are dominated by the charge of the added protons. Thus, before isotope- and isotone-shift data can be compared on an equivalent basis, the charge distribution of the added protons must first be considered. Elastic electron scattering experiments -Fig. 12- have shown that the radial dependence of $\Delta\rho(r)$ between $1f_{7/2}$-shell isotones is well described by $1f_{7/2}$-shell harmonic oscillator wave functions. As a zeroth-order approximation, we therefore calculated a set of $1f_{7/2}$-shell isotone shifts considering only the charge distribution of the added protons. In Fig. 15 the experimental isotone shifts are compared with a harmonic oszillator shell model calculation.

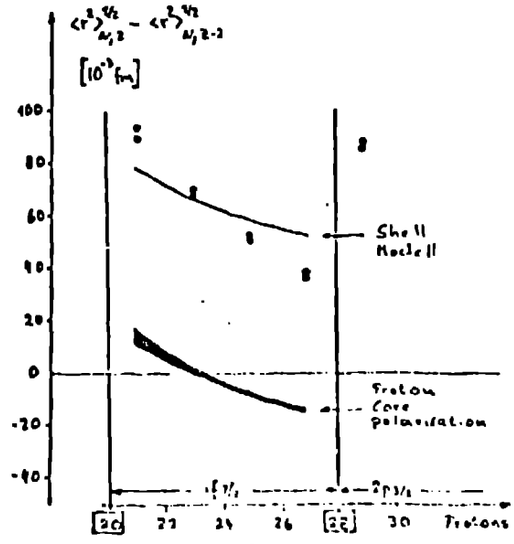

Fig. 15

The actual isotone shifts decrease more rapidly with increasing Z than the calculation would suggest.

It is evident that the effect of the added nucleons on the proton core must be included when considering either isotone or isotope shifts. In the case of isotope shifts, this "core polarisation" is the only effect between N=20 and N=28 (see Fig.4).The difference between the measured isotone shifts and the contribution of the proton charge should be the proton produced core polarisation, (see Fig. 15).This proton core polarisation is positiv in the first half of the $1f_{7/2}$ proton shell and negitive in the second half. The core polarisation caused by the added neutrons, as seen in Fig.4, is in the average about two times stronger than the proton produced core polarisation. We conclude that the proton- and neutron-core polarisation reveal qualitatively a similar behaviour in the $1f_{7/2}$shell.

5.4 Isotone and Isotope odd-even staggering

Around N=50 Fig.16 displays the odd-even staggering for isotones and isotopes. The increase of the RMS-radius due to the first unpaired nucleon is smaller compared to the effect of the second nucleon; this is shown for neut[illegible]

Isotone and Isotope Odd-Even Staggering

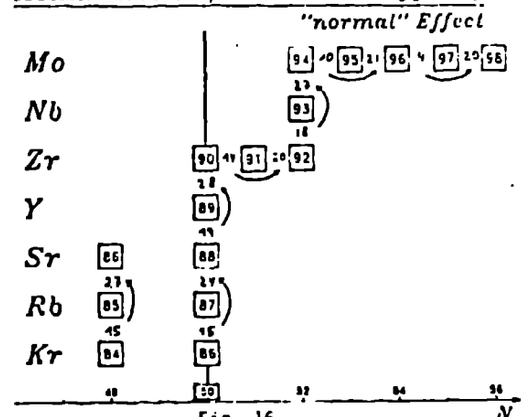

Fig. 16

This may be called the "normal" odd-even staggering effect.Reehal and Sorenson predict smaller deformations for odd then for even isotopes, because ground state correlations are blocked by the unpaired nucleon(18). The arrow in Fig.16 indicates the direction from smaller to larger increase of the RMS-radius.In Fig.17,the isotope odd-even staggering around N=28 shows for N=28 a "normal" effect. The isotone effect is "normal" below Z=28,but for Z=28 the first proton (^{63}Ca-^{62}Ni) yields almost the same increase of the RMS-radius as the second proton (^{64}Zn-^{63}Cu) in the new $2p_{3/2}$ proton shell. The Ca isotope shift in the first half of the $1f_{7/2}$ shell is "normal", whereas in the second half of the $1f_{7/2}$ shell the Ca and Ti shifts for the first added neutron (^{45}Ca-^{44}Ca; ^{47}Ti-^{46}Ti) is larger in the amount of the difference of the RMS-radius compared to the effect of the second neutron (^{46}Ca-^{45}Ca; ^{48}Ti-^{47}Ti). The "normal" odd-even staggering effect in the first half of the $1f_{7/2}$ neutron shell may be explained by the increasing deformation and the "not normal" effect in the second explained by the decreasing deformation. The details of this behaviour, however, may not be easy to explain.

Isotone and Isotope Odd-Even Staggering

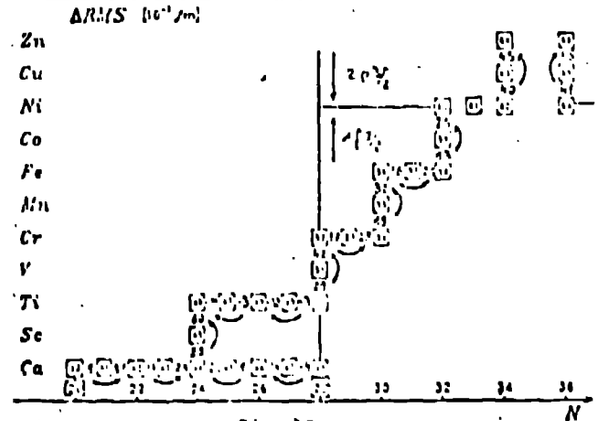

Fig. 17

5.5. Differences of charge distributions and deformation effects

From the Fe, Ni and Zn charge distributions measured by elastic electron scattering one can deduce the change in the half-density radius Δc and the change in the nuclear skin thickness Δt. The result in Fig. 18 shows that Δc is almost constant whereas Δt is decreasing if the neutron shell is more and more filled with neutrons.

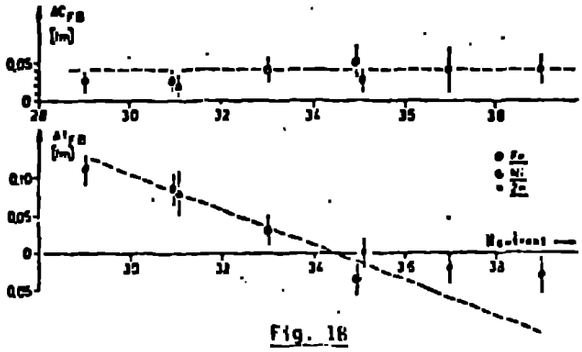

Fig. 18

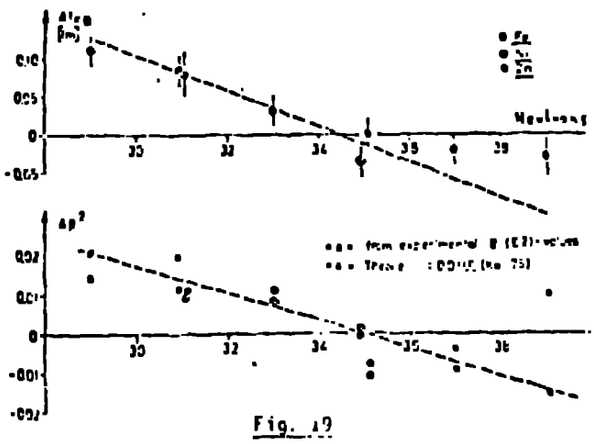

Fig. 19

This tendency is compared in Fig. 19 with the quadrupole deformation changes $\Delta\beta^2$. The similar behaviour of Δt in respect to $\Delta\beta^2$ is obvious and supports the explanation of the isotope shifts by quadrupole deformations, see chapter 5.1.

A new electron scattering measurement of the difference of the ^{48}Ca-^{40}Ca isotopes shows -Fig.20- that some charge is shifted from the inner and outer part of the nucleus to the surface region. This complex structure may be the reason why the isotone shifts in the Ca isotopes can not only be explained by quadrupole deformations and that octupole deformations have also to be considered.

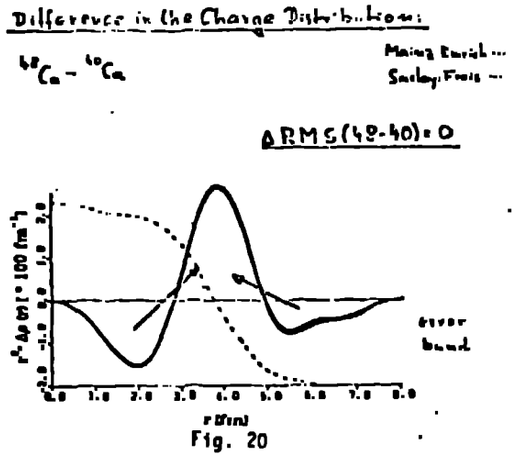

Fig. 20

References:

(1) H.D. Wohlfahrt, O. Schwentker, G. Fricke, H.G. Andresen and E.B. Shera; P.R.C. 22(1980)264

(2) B. Dreher; Phys.Rev.Lett. 35(1975)716

(3) H. Rothhaas; Thesis, Universität Mainz, 1976

(4) H. von der Schmitt; KPH-Report 24/74, Universität Mainz, 1974

(5) E.B. Shera, E.T. Ritter, R.B. Perkins, G.A. Rinker, L.K. Wagner, H.D. Wohlfahrt, G. Fricke and R.M. Steffen; Phys.Rev. C14(1976)731

(6) H.D. Wohlfahrt, E.B. Shera, M.V. Hoehn, Y. Yamazaki, G. Fricke and R.M. Steffen; Phys.Lett. Vol 73B, No. 2(1978)131

(7) H.D. Wohlfahrt, E.B. Shera, M.V. Hoehn, Y. Yamazaki and R.M. Steffen; Phys.Rev. C23(1981)533

(8) L. Schellenberg, B. Robert-Tissot, K. Kaser, L.A. Schaller, H. Schneuwly, G. Fricke, S. Gluckert, G. Mallot and E.B. Shera; Nucl.Phys. A333(1980)333

(9) B. Dreher, J. Friedrich, K. Merle, H. Rothhaas and G. Lührs; Nucl.Phys. A235(1974)219

(10) R.C. Barrett; Phys.Lett. 33B(1970)388

(11) H.R. Collard, L.B.R. Elton and R. Hofstadter; Nucl.Radii in Landolt-Bornstein, Group I, Vol.2

(12) R. Hofstadter; Rev.mod.Phys. 28(1956)214

(13) T. de Forest, Jr. and J.D. Walecka; Advances in Phys. 15(1966)1

(14) H. Ehrenberg, H. Averdung, B. Dreher, G.Fricke, H. Herminghaus, R. Herr, H. Hultzsch, G. Lührs, K. Merle, R. Neuhausen, G. Noldeke, H.M. Stolz, V. Walther and H.D. Wohlfahrt; Nucl. Instr. and Meth 105(1972)253

(15) G. Stephan; KPH-Report 71/3, Universität Mainz, 1971

(16) R. Steiner, K. Merle and H.G. Andresen; Nucl.Instr. and Meth. 127(1975)11

(17) J. Bonn et al.; Zeitschr.f.Physik A 276(1976)203

(18) B.S. Reehal and R.A. Sorensen; Nucl.Phys. A161(1971)[illegible]